

## Sine sweep effect on specimen modal parameters characterization

Nicolas Roy<sup>\*1</sup>, Maxime Violin<sup>2a</sup> and Etienne Cavro<sup>3b</sup>

<sup>1</sup>Top Modal, 130 rue Galilée, 31670 Labège, France

<sup>2</sup>Airbus Defence & Space, 31 rue des Cosmonautes, 31500 Toulouse, France

<sup>3</sup>Intespace, 2 rond-point Pierre Guillaumat, 31029 Toulouse, France

(Received November 21, 2016, Revised February 3, 2017, Accepted March 27, 2017)

**Abstract.** The sine sweep base excitation test campaign is a major milestone in the process of mechanical qualification of space structures. The objectives of these vibration tests are to qualify the specimen with respect to the dynamic environment induced by the launcher and to demonstrate that the spacecraft FE model is sufficiently well correlated with the test specimen.

Dynamic qualification constraints lead to performing base excitation sine tests using a sine sweep over a prescribed frequency range such that at each frequency the response levels at all accelerometers, load cells and strain gages is the same as the steady state response. However, in practice steady state conditions are not always satisfied. If the sweep rate is too high the response levels will be affected by the presence of transients which in turn will have a direct effect on the estimation of modal parameters.

A study funded by ESA and AIRBUS D&S was recently carried out in order to investigate the influence of sine sweep rates in actual test conditions. This paper presents the results of this study along with recommendations concerning the choice of methods.

**Keywords:** sine sweep; FRF estimation; modal identification

---

### 1. Introduction

When performing sine vibration tests with high sweep rates, the response will no longer be stationary (steady state) resulting in a modification of the response envelope due to transient behavior. This could have a direct effect on the identification of the underlying modal parameters.

The effect of the sine sweep rate on modal parameters was first studied analytically using the single degree of freedom (SDOF) model (Hawkes 1964, Cronin 1968, Lollock 2002, Girard and Bugeat 2004, Lalanne 2009, Roy and Girard 2012). From these studies the perturbations in natural frequency, damping and amplitude (modal effective parameters) as a function of the sweep rate could be quantified.

However, these simulations do not take into account other important factors related to sine

---

\*Corresponding author, E-mail: [nicolas.roy@topmodal.fr](mailto:nicolas.roy@topmodal.fr)

<sup>a</sup>E-mail: [maxime.violin@airbus.com](mailto:maxime.violin@airbus.com)

<sup>b</sup>E-mail: [etienne.cavro@intespace.fr](mailto:etienne.cavro@intespace.fr)

vibration tests such as the actual characteristics of the sine sweep excitation generated by the vibration control system and the influence of notching. In addition, the use of more representative models is also necessary to better assess the influence of modal coupling and possible nonlinearities on the swept responses.

Therefore, a study was funded by ESA and AIRBUS D&S (Violin 2015) in order to investigate the influence of sine sweep rates in actual test conditions. The work was organized in three parts:

Creation of representative sine sweep inputs including simulated and measured profiles using the test facilities at INTESPACE. Various sweep rates with and without notching were considered.

- Evaluation of FRF estimation methods on simple models including narrow band and wide band techniques as well as the influence of nonlinearities.

- Evaluation of the FRF estimation methods with industrial cases using FE simulation and test measurements.

This paper presents the work performed in each part of the study along with the findings and recommendations concerning the use of estimations methods to obtain the most reliable modal parameters in the context of sine sweep testing.

## 2. Sine sweep excitation

### 2.1 Numerical simulation procedure

A sine sweep excitation  $\ddot{u}(t)$  of unitary amplitude can be defined using Eq. (1) where  $f(t)$  is the instantaneous frequency which depends on the specific sweep type defined below.

$$\ddot{u}(t) = \sin \left[ 2\pi \int_0^t f(\tau) d\tau \right] \quad (1)$$

The three most common sweep types are linear, exponential and hyperbolic. The corresponding frequency functions  $f(t)$  are plotted and defined in Fig. 1.

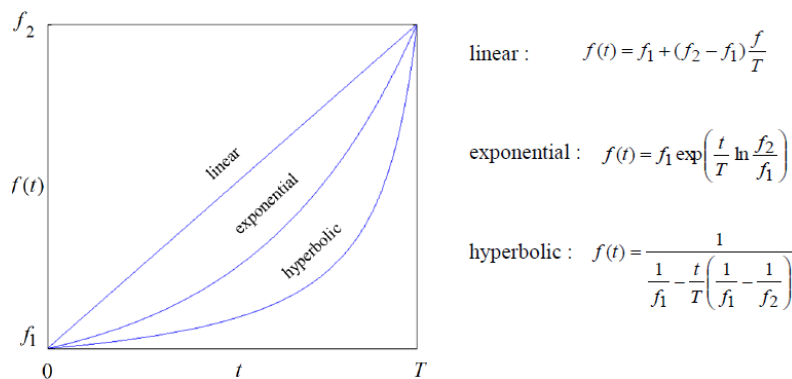


Fig. 1 Sine Sweep Types

The exponential sweep is often used for spacecraft vibration testing. The exponential sweep

rate is usually expressed through the parameter  $R$  given in oct/min and which indicates that after each minute the excitation frequency is multiplied by  $2^R$ . The value of  $R$  is obtained by the following expression.

$$R = \frac{\ln(f_2 / f_1)}{\ln(2)} \frac{60}{T} \quad (2)$$

When a SDOF system is excited by a sine sweep, the response amplitude envelope will deviate more or less from the steady state amplitude due to the effects of transients. This is illustrated in Fig. 2 for a mode having natural frequency 20 Hz and 1% damping ratio and a positive sweep rate of 4 oct/min.

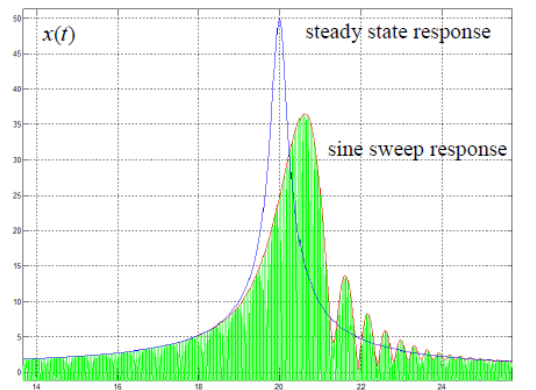


Fig. 2 Effect of Sine Sweep on SDOF Response

We see that the shape and position of the resonant peak are altered as a function of the sweep rate and direction. Moreover, a beat pattern or "ringing" following the main peak occurs. This ringing is a result of the system responding at two frequencies of nearly the same value comprising the transient response at the natural frequency and the harmonic response at the swept excitation frequency.

In general, a sine sweep will *decrease* the amplitude of the peak, *shift* the position of the peak (along the direction of the sweep), *broaden* the peak width and *distort* the shape of the peak. The higher the sweep rate, the more these effects are accentuated.

The non-dimensional parameter  $\eta$  can be used to quantify the deviation of the sine sweep response from the steady state response. It is defined as follows where  $Q$  is the quality factor  $1/(2\zeta)$  and  $N$  the number of cycles of excitation within the half-power points of the steady state response.

$$\eta = Q / N \quad (3)$$

As  $\eta$  increases in value the sine sweep response deviates from the steady state response. The ratio of the swept amplitude to the steady state amplitude versus  $\eta$  obtained by Roy and Girard (2012) is plotted in Fig. 3. For small values of  $\eta$  ( $\eta < 0.1$ ) the swept response level is very close to steady state.

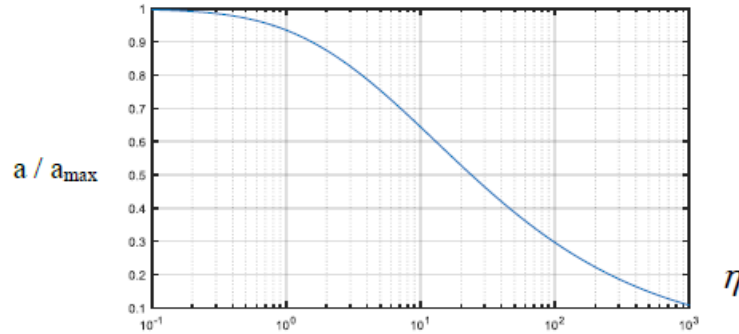


Fig. 3 Fraction of Steady State Amplitude

For an exponential sweep, the value of  $\eta$  is defined as follows (Lalanne 2009).

$$\eta = \frac{Q^2 R \ln(2)}{60 f_k} \quad (4)$$

Using Eq. (4) for the example of Fig. 2, we obtain  $\eta \approx 5.8$  which confirms the strong deviation from steady state.

Further examining Eq. (4) we notice that  $\eta$  is proportional to  $Q^2$  and inversely proportional to the natural frequency  $f_k$ . This means that for a given sweep rate, the low frequency modes with low damping will be more influenced by the sine sweep.

It is interesting to note that the dependence on the natural frequency  $f_k$  in Eq. (4) can be eliminated by considering a hyperbolic sweep instead of an exponential sweep. The expression for  $\eta$  for a hyperbolic sweep is provided below.

$$\eta = \frac{Q^2 \left( \frac{1}{f_1} - \frac{1}{f_2} \right)}{T} \quad (5)$$

The hyperbolic sweep will therefore produce the same deviation from steady state response at all frequencies for modes with a given damping. This could be a useful alternative to the exponential sweep especially when the first modes are close to the lower frequency limit  $f_1$ .

## 2.2 Sine sweep inputs

Measured sine sweep inputs were obtained at INTESPACE using a 80 kN shaker in an unloaded configuration with a tri-axial accelerometer installed directly at the free interface.

Two control systems were used-LMS and Spectral Dynamics. The characteristics of each system are summarized in Fig. 4. The Nicolet acquisition system was used because the Spectral Dynamics console was not able to acquire time histories.

The following test parameters were considered:

Sweep type: exponential from 5 to 100 Hz  
 Sweep rate: 1, 2 and 4 octaves/min

	LMS	Spectral Dynamics
Piloting	LMS	Spectral Dynamics
Acquisition	LMS	Nicolet (32 channels)
Sampling frequency	12 800 Hz	10 000 Hz

Fig. 4 Description of Control Systems

Sweep direction: ascending and descending  
 Sweep profile: constant (1 g) and notched  
 The notched profile specification is shown in Fig. 5.

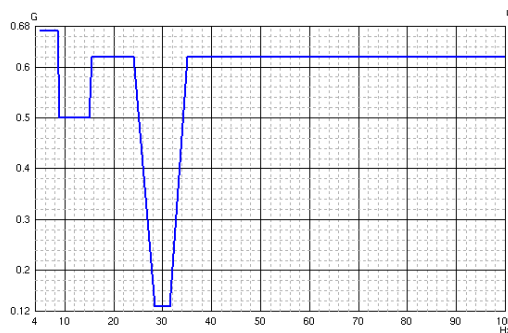


Fig. 5 Notched Profile

A total of 24 test runs were performed using various combinations of the control systems and test parameters. The tests are itemized below in Fig. 6.

The measured sine sweep inputs are plotted in Fig. 7 for the test pair T9/T21. The other inputs show similar characteristics. Measurements from the LMS system appear to better reproduce the specified profile compared to the Spectral Dynamics inputs.

We notice that the Spectral Dynamics measurements do not start at time zero. This is because the system needs a certain amount of time to reach the specified level and that the acquisition had to be triggered manually.

Also, perturbations in the signal due to electrical interference were present in some of the Spectral Dynamics measurements. However, these perturbations concentrated at 50 Hz and its harmonics had little impact on subsequent analyses.

### 3. FRF estimation methods

#### 3.1 Introduction

Two types of methods were considered for estimating the FRF from sine sweep responses:

1. Narrow Band (or Local) methods which determine the FRF at a given frequency (time) by considering only the portion of the measurements near the frequency (time) in question.
2. Wide Band (or Global) methods which determine the FRF at all frequencies by

TEST	Control system	Profile	Sweep rate (oct/min)	Sweep direction
T1	LMS	Constant	1	+
T2		Constant	1	-
T3		Constant	2	+
T4		Constant	2	-
T5		Constant	4	+
T6		Constant	4	-
T7		Notched	1	+
T8		Notched	1	-
T9		Notched	2	+
T10		Notched	2	-
T11		Notched	4	+
T12		Notched	4	-
T13	SD	Constant	1	+
T14		Constant	1	-
T15		Constant	2	+
T16		Constant	2	-
T17		Constant	4	+
T18		Constant	4	-
T19		Notched	1	+
T20		Notched	1	-
T21		Notched	2	+
T22		Notched	2	-
T23		Notched	4	+
T24		Notched	4	-

Fig. 6 Test Runs for Sine Sweep Inputs

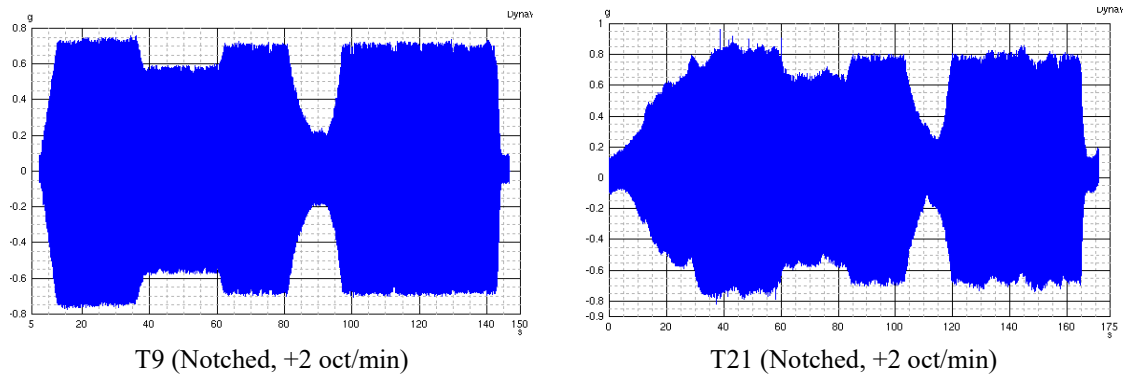


Fig. 7 Comparison of Sine Sweep Inputs

considering the entire time history of measurements.

### 3.2 Narrow band methods

Narrow band methods such as the Co-Quad analyzer, Tracking filter and Hilbert transform are simple to implement and in some cases can be performed in real-time during the vibration test. As illustrated in Fig. 8, the general idea behind these methods is to compare the response to the excitation near a given frequency  $f$  in order to determine the amplitudes  $X$  and  $Y$  and phase shift  $\theta$ . This leads directly to the FRF expressed as  $H(f) = \frac{Y}{X} e^{i\theta}$ . In practice the measurements are filtered beforehand to remove unwanted harmonics.

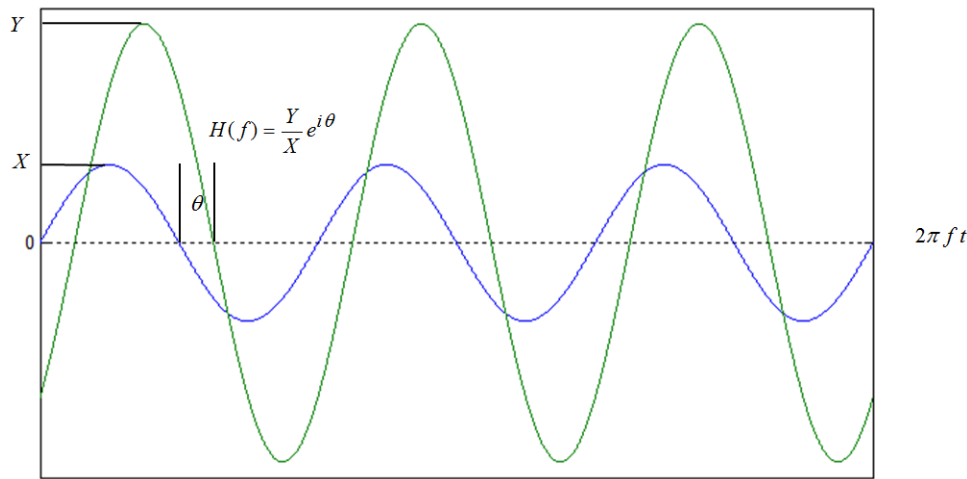


Fig. 8 Illustration of Narrow Band Methods

The principal drawback with narrow band methods is that they all assume steady-state conditions for the response at each given frequency. As shown previously, this assumption is valid only for very slow sweep rates (i.e. small values of  $\eta$ ), and therefore narrow band methods will produce FRF with the same errors described in Section 2.1.

### 3.3 Wide band methods

Wide band methods do not rely on the steady-state assumption since the FRF are determined by means of the Fourier Transform applied to the entire excitation and response time histories. For short duration transients with zero starting and ending values, the FRF can be obtained using the Discrete Fourier Transform (DFT) or Fast Fourier Transform (FFT) of the excitation and response as shown below.

$$H(\omega) = \frac{FT(y(t))}{FT(x(t))} = \frac{Y(\omega)}{X(\omega)} \quad (6)$$

However, sine sweep signals have relatively long durations with initial and final conditions which are not necessarily zero. In this case it is better to estimate the FRF from the spectral density

functions  $S_{xx}(\omega)$ ,  $S_{xy}(\omega)$  and  $S_{yy}(\omega)$ . This leads to the following expressions for the FRF estimators  $H_1(\omega)$  and  $H_2(\omega)$  and the coherence function  $\gamma^2(\omega)$ .

$$H_1(\omega) = \frac{S_{xy}(\omega)}{S_{xx}(\omega)} \quad H_2(\omega) = \frac{S_{yy}(\omega)}{S_{yx}(\omega)} \quad \gamma^2(\omega) = \frac{H_1(\omega)}{H_2(\omega)} \quad (7)$$

To minimize the effect of noise, averaging of the spectra is performed before computing the FRF using Eq. (7). Two types of spectral averaging techniques can be employed: time averaging and frequency averaging.

In this study we considered Welch's method for time averaging of spectra. This technique is often used with stationary random processes in order to minimize the statistical error (variance). However, in the context of sine sweep excitations, Welch's method can still be used to reduce noise as shown by Orlando, Peeters and Coppotelli (2008). Time averaging consists of decomposing the excitation and response time histories into overlapping segments as depicted in Fig. 9. Each time segment is weighted (convolved) with a window function (Hamming, Han, Welch, etc.) to minimize leakage. The spectra are then calculated for each weighted segment and then averaged together.

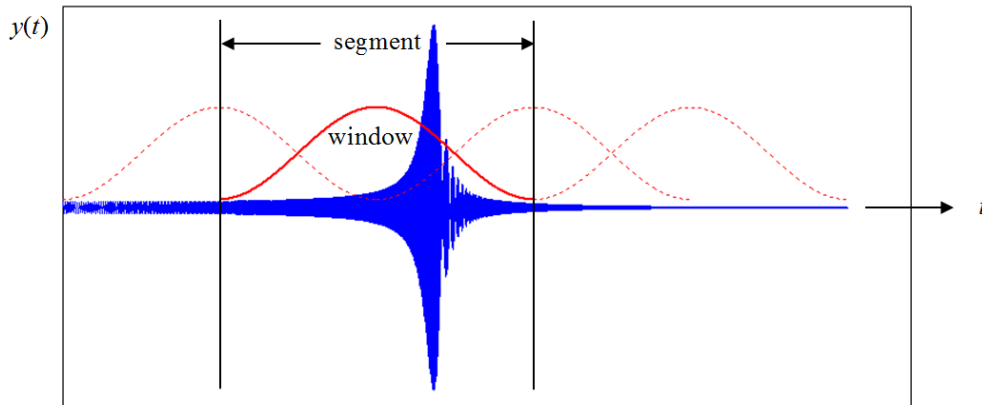


Fig. 9 Time averaging using Window Segments

Frequency averaging is performed by averaging groups of frequency points of the spectral density functions according to Otnes and Enochson (1978). The idea is to introduce a spectral density expressed over a reduced number of frequency values  $S(k)$  where each frequency value represents the average value of the neighboring points of the initial spectrum. For example, if we wish to reduce the number of frequency points by a factor of  $2N$  then the following averaging formula can be used.

$$S(k) = \frac{1}{2N} \left[ \frac{1}{2} G(k-N) + \frac{1}{2} G(k+N) + \sum_{j=-N+1}^{N-1} G(k+j) \right] \quad (8)$$

This technique is illustrated in Fig. 10 for the case of  $N=2$  (reduction by a factor of 4).

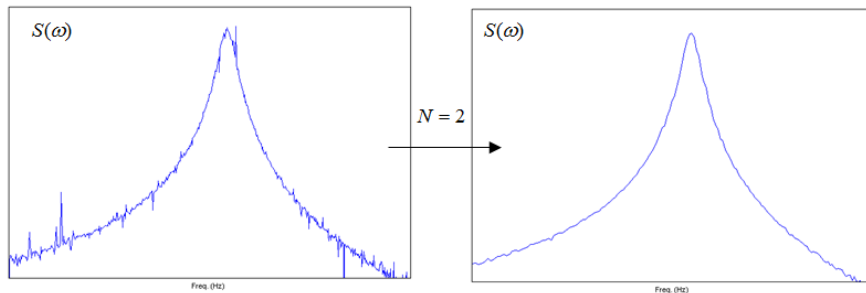


Fig. 10 Frequency Averaging of Spectral Density Functions

### 3.4 Evaluation strategy

FRF estimators using narrow band (local) and wide band (global) methods were considered. The work was carried out according to the steps shown below in Fig. 11 and is described hereafter.

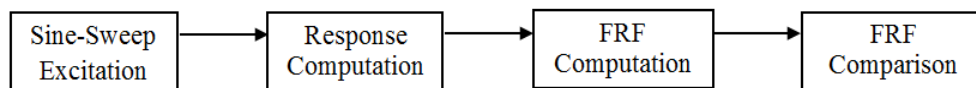


Fig. 11 Flowchart for Evaluation of FRF Estimators

Measured sine sweep inputs (Section 2.2) as well as simulated excitations were considered.

The time history responses were computed analytically using simple models via mode superposition techniques. Numerical integration was performed using recurrence formulas based on Duhamel's integral (Craig 1981) assuming a piecewise-linear excitation and a constant time step equal to the inverse of sampling frequency. All calculations were performed with MATLAB®.

Two types of models were considered:

1. **DIRECT INPUT** - the modal parameters (natural frequency, damping and effective transmissibilities) are defined directly for any number of modes.

2. **SPOT 6** - The modal parameters are obtained from a Craig-Bampton (condensed) model of the SPOT 6 S/C provided by Airbus D&S. The model comprises 22 modes from 0.25 to 36 Hz with modal damping in the range of  $0.02 \leq \zeta_k \leq 0.12$  ( $4 \leq Q_k \leq 25$ ).

The FRF were computed using standard codes available at INTESPACE (DynaWorks® and LMS) and using wide band methods developed in MATLAB.

The comparison of the FRF obtained from the different inputs, models and methods are presented hereafter.

### 3.5 FRF using narrow band methods

FRF computation using DynaWorks and LMS was performed for various sine sweeps and models. The algorithm used by DynaWorks is based on a narrow band (local) approach. The principal computational steps are described below.

1. **Computation of the frequency table.** This function uses Prony analysis to determine the excitation frequencies from the input measurement.

2. *Signal resampling.* This function uses a cubic spline technique to resample the output measurements at the frequencies of the frequency table.

3. *Computation of the FRF.* From the resampled input and output time histories, this function computes either the harmonic (fundamental) FRF by DFT filtering or the global FRF by time averaging. The harmonic FRF provide both amplitude and phase whereas the global FRF are amplitude only.

Information concerning the algorithm used by LMS was not available. However the FRF obtained with LMS were consistent with a narrow band approach.

As an example, the FRF shown in Fig. 12 were computed using the SDOF model with a mode at 20 Hz with 1% damping. The FRF computed using the LMS constant profile with a sweep rate of 1 oct/min are shown at left whereas the FRF using the LMS notched profile with a negative sweep rate of -2 oct/min are shown at right. The FRF obtained from DynaWorks and LMS are compared with the steady state response.

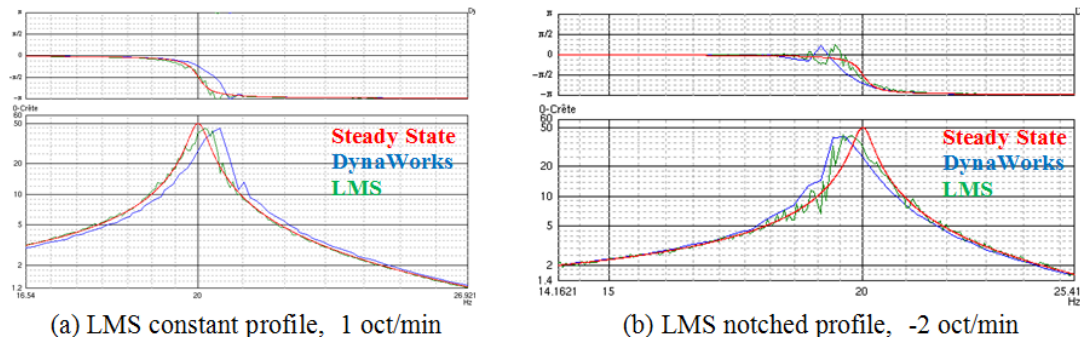


Fig. 12 Comparison of FRF obtained from DynaWorks and LMS

The shifts in frequency and decrease in amplitude are consistent with predictions based on narrow band methods. The deviation from the steady state response is more pronounced using the higher sweep rate of -2 oct/min. The FRF computed with LMS are somewhat noisy. This is because the pilot accelerometer was used for the reference signal instead of the DRIVE or COLA signals.

### 3.6 FRF using wide band methods

The first comparison was carried out using a SDOF model with a natural frequency of  $f_k = 26$  Hz and a damping of  $Q_k = 50$ . The natural frequency of 26 Hz was chosen such that the resonant peak is located in the slope of the notching profile. The following positive and negative sweep rates with and without notching were considered:

- +1 oct/min, without notching, simulated with MATLAB
- 2 oct/min, without notching, simulated with MATLAB
- +4 oct/min, notched, using LMS system
- 4 oct/min, notched, using Spectral Dynamics system

No averaging techniques were used to compute the FRF. The FRF for the -4 oct/min sweep rate is shown in Fig. 13 alongside the corresponding response time history. The FRF for the other cases

are nearly identical and display very little noise even with no averaging. The error between the computed FRF and the theoretical FRF of the model is negligible. Therefore, for this comparison, the use of the wide band method preserves the modes of the model even when using high sweep rates with or without notching.

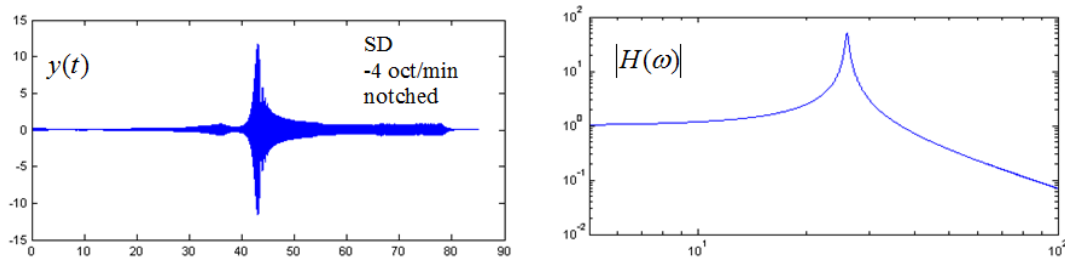


Fig. 13 FRF using Wide Band Method on SDOF Model

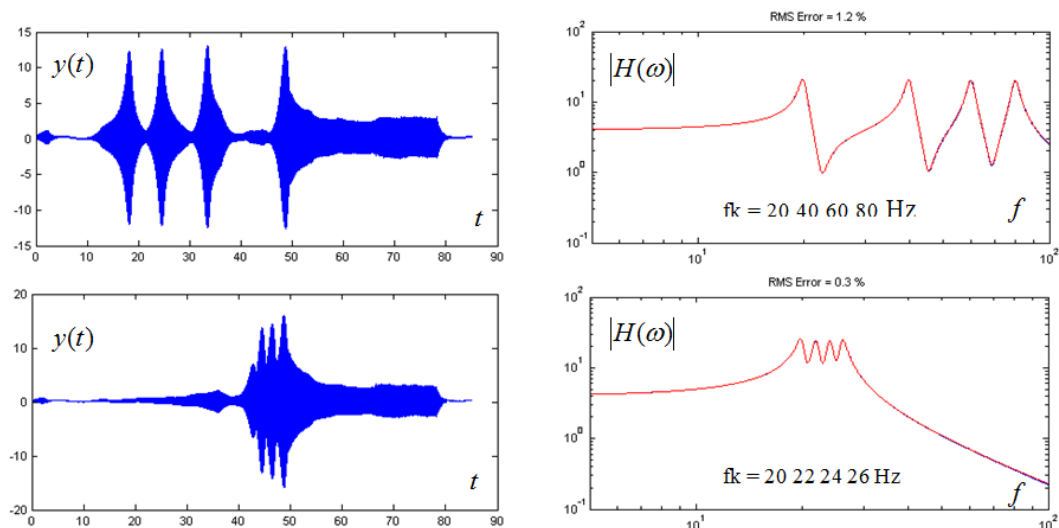


Fig. 14 FRF using Wide Band Method on Closely Spaced Modes

In order to evaluate the effect of coupling between modes on the FRF, 2 models with 4 modes were considered with different modal densities:

Model 1: widely spaced natural frequencies at 20, 40, 60 and 80 Hz

Model 2: closely spaced natural frequencies at 20, 22, 24, and 26 Hz

For both models a constant damping of  $Q_k = 20$  was used along with unit effective transmissibilities. No averaging techniques were used. The Spectral Dynamics notched sine sweep at  $-4$  oct/min was used for the excitation.

The results are presented below in Fig. 14. The theoretical FRF (red curve) are plotted on top of the calculated FRF (blue curve). The rms error between the two curves is shown at the top of the plots and is shown to be less than or equal to 1%.

FRF were computed using the SPOT 6 condensed model at the following response points:

Node 11314 along the x-axis

Node 4330003 along the x-axis

A simulated sine sweep rate of  $-4$  oct/min without notching was used as the excitation. Again no averaging was performed on the FRF. The response time histories and corresponding FRF are plotted in Fig. 15. Here again we see very little differences between the calculated and theoretical FRF ( $< 1\%$  rms)-even near the anti-resonances.

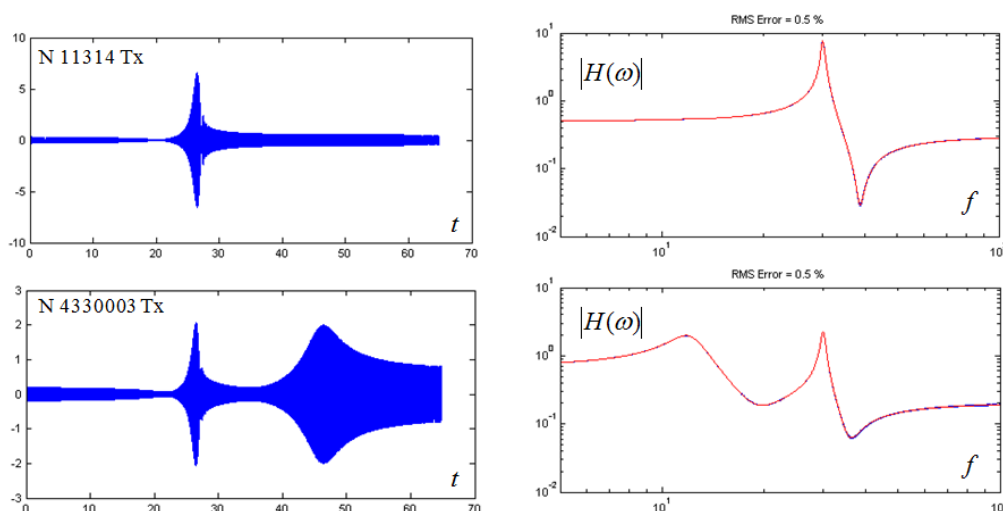


Fig. 15 FRF using Wide Band Method on SPOT 6 Condensed Model

In the previous cases, averaging was not required when computing the FRF due to the absence of noise in the simulated responses. In the presence of noise, averaging techniques will smooth out the FRF, but will also perturb the shape of the FRF and therefore the associated modal terms.

To evaluate the averaging techniques noise was added to the responses. The FRF were then recomputed using time domain and frequency domain averaging techniques. The following observations were formulated based on the results.

When no averaging is performed, noise is present at all frequencies of the FRF, however the calculated FRF shows no visible biased error with respect to the theoretical FRF.

Using Welch's method, the calculated FRF are smoother, however the averaging reduces the amplitude of the peak and therefore alters the modal properties, and in particular the damping and effective parameters. The degree to which the FRF and modal properties are modified depends on the choice of segments, window type and overlap.

Using frequency averaging, the calculated FRF are smoother and appear to be less altered compared to Welch's method.

### 3.7 Influence of nonlinearities

The above FRF comparison was carried out using a linear model with mode superposition techniques. In reality, structures often exhibit nonlinear behavior to one degree or another. Sources

of nonlinearities are wide ranging and include boundary (contacts), geometry (large displacements) and material (plastic and viscoelastic) nonlinearities.

The presence of nonlinearities can have a strong influence on the dynamic response of a structure including changes in resonance, occurrence of harmonics, instabilities and even chaotic behavior. It is therefore of interest to examine the influence of nonlinearities in the estimation of FRF.

To do so, the SDOF model shown in Fig. 16 with a nonlinear restoring force  $\varphi(x) = k(1 + \mu x^2)x$  was considered. Although this model is fairly simple and limited to a particular type of nonlinearity it does illustrate the various effects on the dynamic responses and FRF estimation methods.

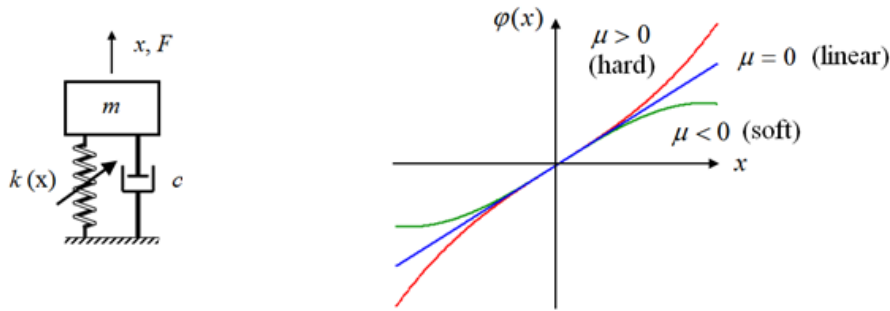


Fig. 16 Nonlinear SDOF Model

The corresponding equation of motion known as the Duffing equation is shown below in Eq. (9).

$$m\ddot{x} + c\dot{x} + k(1 + \mu x^2)x = F \quad (9)$$

The effect of the nonlinear stiffness on the frequency response of the model is illustrated in Fig. 17 for the case of a hardening spring ( $\mu > 0$ ). We see a significant change in the position, amplitude and shape of the resonance.

Another major difference between the linear and nonlinear systems is that the latter are multi-valued at certain frequencies. In the region between the two arrows there are three different response levels at a given excitation frequency. This is a consequence of the cubic nature of the stiffness. In the case of a sine sweep excitation this leads to a jump phenomenon or instability as the response amplitude changes (jumps) suddenly from one value to another for an incremental change in excitation frequency.

In addition to the primary resonance, secondary resonances particular to the nonlinear model can appear. These resonances referred to as nonlinear resonances or harmonics occur at odd multiples of the excitation frequency. Fig. 18 shows the steady state behavior of the above nonlinear system (but with  $c = 0.02$ ) excited at  $\omega = \omega_0/3 = 1/3$ . The time history shows a higher harmonic “rider” on top of the forcing frequency which is about three times the excitation. In other words an excitation far from resonance appears to excite resonance.

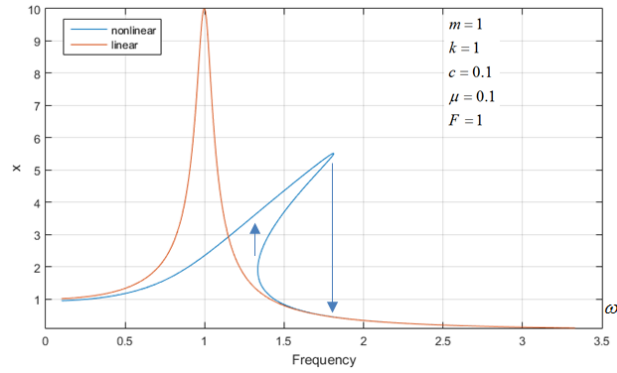


Fig. 17 Frequency Response Behavior on Nonlinear Model

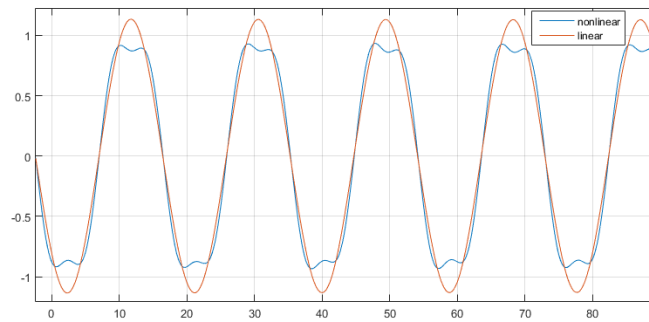


Fig. 18 Response away from Resonance

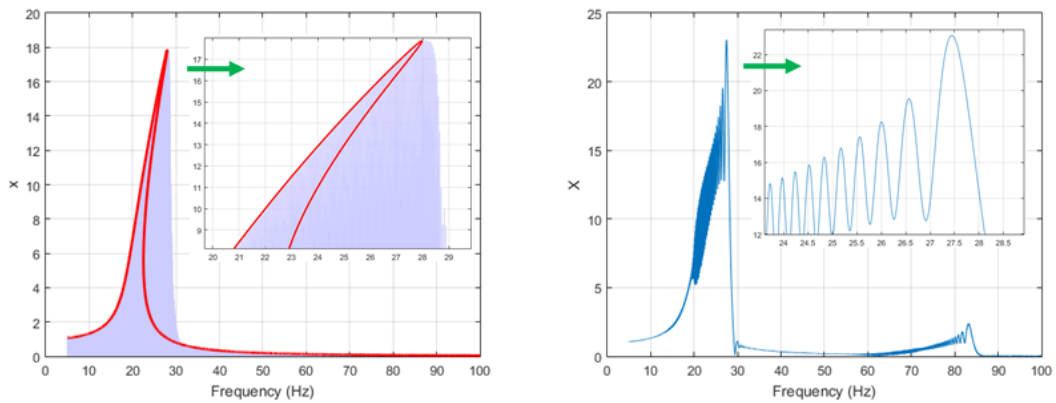


Fig. 19 Nonlinear Response (left) and FRF (right)

The responses of the nonlinear SDOF model to a sine sweep excitation were computed using numerical integration. Several cases were investigated with different sweep rates and directions, damping and levels of nonlinearity. One case with significant nonlinear behavior is shown below in Fig. 19. The FRF shows significant rippling to the left of the peak and reproduces the jump to the right of the peak. The contribution of the harmonics appears to be spread over a higher frequency range with increased amplitude.

### 3.8 Conclusions on FRF methods

Based on the above comparison of FRF using different sine sweep inputs, models and FRF extraction techniques the following conclusions and recommendations can be made.

Narrow band (local) methods should not be used to estimate FRF from sine sweep tests unless the sweep rate is small enough to ensure steady-state behavior.

Wide band (global) methods based on the Fourier Transform provide a reliable estimation of FRF and are insensitive to sweep rate and notching.

Averaging methods (Welch and frequency averaging) can be used to reduce the influence of noise. However, averaging can modify the shape of the FRF peaks and the associated modal parameters. In many cases, frequency averaging seems to better preserve the shape of the FRF peaks compared to time averaging (Welch).

In the presence nonlinearities, global methods can lead to significantly degraded FRF estimations due to the presence of instabilities and harmonics which can produce peaks that are not associated with modes. In this case the use of local methods may be more robust despite the limitations regarding steady state conditions.

## 4. Industrial test cases

### 4.1 Introduction

The FEM of the SPOT6/ASTROTERRA spacecraft shown in Fig. 20 was used as an industrial test case for this study. The S/C is in sine test configuration (empty tanks, stowed solar arrays) and is clamped at the launcher/spacecraft interface. The Z axis is the longitudinal axis of the S/C.

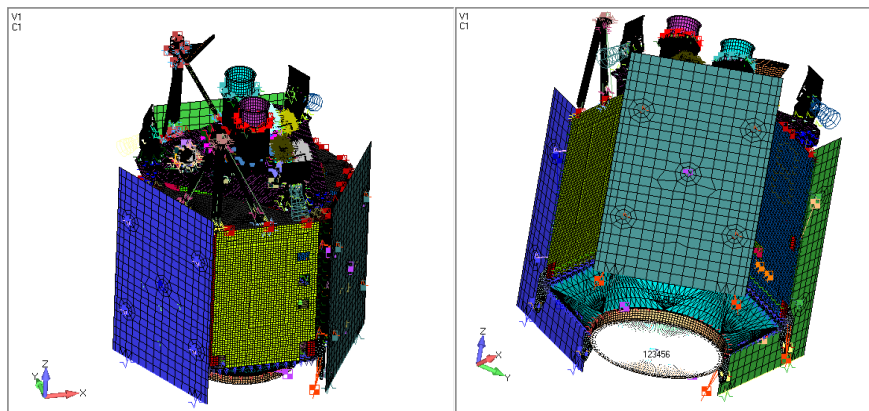


Fig. 20 SPOT6/ASTROTERRA FEM

The first step was to compute reference FRF using MSC/NASTRAN with modes up to 400 Hz in order to be representative in the 5-100 Hz frequency range. Modal damping consistent with test predictions was used. A constant base acceleration of  $1 \text{ m/s}^2$  was imposed along the lateral Y-axis. A response point located on the avionic unit mounted on the PY panel was chosen since it

provided two modes below 50 Hz: a global S/C mode near 30 Hz and a local mode near 45 Hz.

The next step was to compute transient responses in NASTRAN (SOL 112) using the sine sweep inputs presented in Section 2.2 with constant and notched profiles and various sweep rates up to  $\pm 4$  oct/min.

Finally, the FRF were computed using DynaWorks (narrow band method) and wide band methods based on Fourier transform. The two main modes were identified using a SDOF method to evaluate the quality of the FRF.

To complete the industrial application, an additional evaluation of the impact nonlinearities on wide and narrow band methods was performed using test data of a telecom S/C.

#### 4.2 FRF evaluation

The FRF were computed with the narrow band method in DynaWorks for the different sine sweep inputs and compared to the reference (steady state) FRF. The results are shown in Fig. 21 for the case of a high sweep rate (ascending and descending directions).

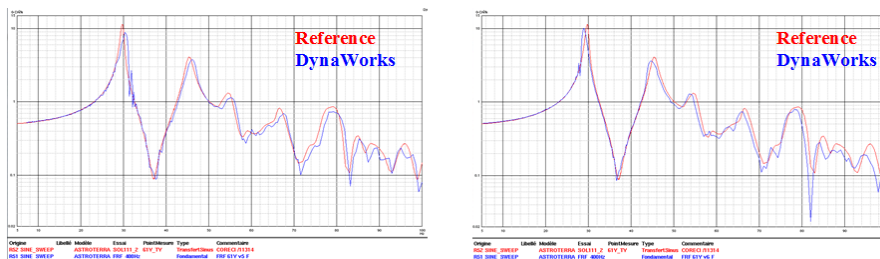


Fig. 21 FRF using DynaWorks Method

Concerning the two main modes, the frequency shift reaches 2% for a sweep rate of  $-4$  oct/min. A 1 Hz shift exists between the ascending sweep of  $+4$  oct/min and the descending sweep of  $-4$  oct/min. This variation can be a concern for the extraction of the modal parameters of S/C main modes found in the low frequency range. A decrease in amplitude occurs up to 20% for a sweep rate of  $+4$  oct/min. As a consequence, the identified modal damping values are higher than the reference values.

The FRF obtained using the wide band methods were nearly identical to the reference FRF for all sweep rates and profiles considered. This is consistent with the findings using the simple models.

#### 4.3 Impact of nonlinearities

The above results do not take into account nonlinear behavior of the S/C such as presence of harmonics coming from a nonlinear joint stiffness. In order to evaluate the impact of nonlinearities on wide and narrow band methods, test data from an Airbus S&D telecom S/C was studied.

Two runs of the test campaign were studied: a low-level constant 0.1g profile with a descending sweep of  $-2$  oct/min between 5 and 150 Hz, and a qualification level notched profile with a descending sweep of  $-3$  oct/min between 5 and 100 Hz.

The FRF were computed for sensors likely to show nonlinear effects using narrow band (DynaWorks) and wide band methods. For the low level run where nonlinear effects are weak, narrow and wide band methods produced similar FRF as shown in Fig. 22. However, for the qualification level run containing strong nonlinearities, the wide band method produces perturbed FRF around resonances. The narrow band method is less sensitive to these nonlinear phenomena.

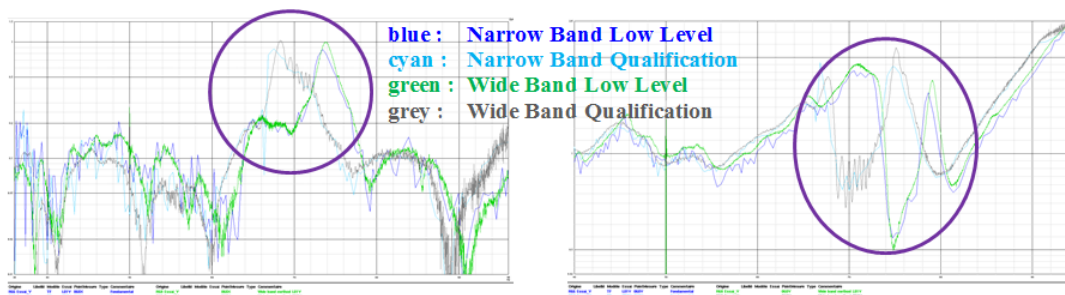


Fig. 22 FRF from Nonlinear Test Data

## 5. Conclusions

This comparative study of FRF extraction techniques on theoretical models and industrial cases leads to the following conclusions.

Narrow band (local) methods available in Dynaworks or LMS are sensitive to the sine sweep rate and may alter the modal parameters identified from the FRF.

Wide band (global) methods based on the Fourier Transform are insensitive to sweep rate and notching.

In the case of a linear system, wide band methods provide a reliable estimation of the FRF but they may lead to disturbed FRF on sensors with strong nonlinear behavior. During future test campaigns, both wide-band and narrow band methods could be of use to estimate FRF. Nevertheless, current practice using narrow band methods should be sufficient to fulfill the objectives of industrial sine test campaigns.

The use of the wide band methods could help to improve several post-processing tasks such as modal identification, FEM updating, and check of the integrity of the structure by comparing two low level test runs.

The narrow band methods should be retained in order to deal with specific sensors with strong nonlinear effects.

The development of a hybrid method based on the wide band method but not sensitive to nonlinearities could be considered for the future.

## 6. References

- Craig, R.R. (1981), *Structural Dynamics-An Introduction to Computer Methods*, John Wiley & Sons.  
 Cronin, D.L. (1968), *Response Spectra for Sweeping Sinusoidal Excitations*, Shock and Vibration Bulletin.  
 Girard, A. and Bugeat, L.P. (2004), "Effect of sine sweep rate on modal parameter identification",

- Proceedings of the 5th International Symposium on Environmental Testing for Space Programmes*, The Netherlands.
- Hawkes, P.E. (1964), *Response of a Single-Degree-of-Freedom System to Exponential Sweep Rates*, Shock and Vibration Bulletin, 33, Part II.
- Lalanne, C. (2009), *Mechanical Vibration & Shock Analysis*, John Wiley & Sons, Vol 1: Sinusoidal Vibrations, 2nd Edition.
- Lollock, J.A. (2002), "The effect of swept sinusoidal excitation on the response of a single-degree-of-freedom oscillator", *Proceedings of the 43rd AIAA Structures, Structural Dynamics, and Materials Conference*, Denver.
- Orlando, S., Peeters, B. and Coppotelli, G. (2008), "Improved FRF estimators for MIMO sine sweep data", *Proceedings of the ISMA 2008 International Conference on Noise and Vibration Engineering*, Leuven, Belgium.
- Otnes, R.K. and Enochson, L. (1978), *Applied Time Series Analysis*, John Wiley & Sons, Vol 1: Basic Techniques.
- Roy, N. and Girard, A. (2012), "Revisiting the effect of sine sweep rate on modal identification", *Proceedings of the European Conference on Spacecraft Structures, Materials and Environmental Testing*, Noordwijk, The Netherlands.
- Violin, M. (2015), *Sine Sweep Effect on Specimen Modal Parameters Characterization*, Executive Summary, AIRBUS D&S, MTF.SWEE.TN.5468, Issue 01, Rev 01.